




Effect of soldering time on the microstructure and mechanical properties of SnBi/SACBN/Cu solder joint

Yang Liu^{1,2}, Jian Chang^{1,3}, Yuxiong Xue^{1,*} , Rongxing Cao¹, Hongxia Li¹, Shu Zheng¹, and Xianghua Zeng¹

¹ College of Electrical, Energy and Power Engineering, Yangzhou University, Yangzhou 225127, People's Republic of China

² Energy and Environment Engineering Institute, Nanchang Institute of Technology, Nanchang 330044, China

³ School of Material Science and Engineering, Harbin University of Science and Technology, Harbin 150040, People's Republic of China

Received: 29 December 2021

Accepted: 23 February 2022

Published online:

9 March 2022

© The Author(s), under exclusive licence to Springer Science+Business Media, LLC, part of Springer Nature 2022

ABSTRACT

To improve the mechanical properties of SnBi solder joints, Sn–Ag–Cu–Bi–Ni (SACBN) bumps were pre-soldered on the Cu pads, and thus the SnBi/SACBN/Cu solder joints were obtained in this work. By comparing with SnBi/Cu, the effects of soldering time on the microstructure and mechanical properties of SnBi/SACBN/Cu solder joint were investigated. Experimental results show that increasing soldering time suppresses the composition segregation in SnBi bulk, but it leads to the coarsening of β -Sn and Bi-rich phases. As the soldering time increases, the interfacial IMC layers in the SnBi/Cu and the SnBi/SACBN/Cu solder joints gradually become thicker. The growth of the $(\text{Cu}, \text{Ni})_6\text{Sn}_5$ interfacial IMC in SnBi/SACBN/Cu is mainly based on solid–solid diffusion. Its growth rate is lower than that of the IMC whose growth is dominantly due to liquid–solid diffusion in SnBi/Cu. The addition of SACBN bulk decreases the hardness of the SnBi bulk. Meanwhile, the hardness shows a decreasing trend as the soldering time increases. When the soldering time is 40 s and 160 s, SACBN bulk suppresses the propagation of fracture in SnBi bulk and improves the shear strength of the solder joint. As the soldering time reaches 280 s, the shear strength of the SnBi/SACBN/Cu solder joint decreases, and the fracture is mainly located in the SnBi bulk.

Address correspondence to E-mail: yxxue@yzu.edu.cn

1 Introduction

SnBi eutectic alloy is widely used in low-temperature soldering in electronic packaging due to its low melting point and low cost [1–3]. However, the high concentration of brittle Bi-rich phase reduces the ductility of the SnBi solder and increases the risk of interface brittle fracture, which seriously affects the reliability of solder joints [4, 5]. Due to the miniaturization and high integration trend of electronic components, the reliability of solder joints is getting increasingly crucial [6–8]. Therefore, improving the performance and reliability of SnBi solder is of great significance.

Alloying a trace amount of additives into the alloy is one of the feasible methods to optimize SnBi solder. Ma et al. [9] added 0.7% Zn nanoparticles into the SnBi solder and soldered them on the Cu substrate to obtain the SnBi–Zn/Cu solder joints. The interfacial reaction and creep resistance of the solder joints during liquid aging were studied. The results showed that the coarsening of the Bi-rich phase and the growth of the Cu–Sn intermetallic compound in the bulk solder are suppressed due to the addition of 0.7% Zn nanoparticles. Cr powders with several weight fractions were doped into SnBi solder by Zhu et al. [10]. The elongation of solder slab and the ultimate tensile strength (UTS) of solder joint were, respectively, enhanced by 56% and 10% when the concentration of Cr was 0.2 wt% in the solder alloy. Meanwhile, the fracture mechanism changed from brittle fracture to ductile fracture in both the solder joint as well as the slab. In addition, other elements, such as Ag, Sb, Mo, Ni, and In, are also considered as the additives for SnBi and are investigated widely [11–14].

Optimizing the surface layer of the solder pad is also an effective way to improve the quality of SnBi solder joint [15–17]. The common surface finish processes on Cu are, for example, Organic Solderability Preservative (OSP), Electroless Nickel/Immersion Gold (ENIG), Hot Air Solder Leveling (HASL), etc. Besides, small amounts of Ag, Al, Sn, or Zn elements are also added into the Cu substrate to modify the performance of SnBi/Cu solder joint [18]. Wang et al. [19] obtained a SnAgCu (SAC) coated layer on the Cu pad through the HASL process. The aged SnBi solder joints on the bare Cu pad showed lower shear strength and brittle failure through the interfacial intermetallic compound (IMC) layer, while the SAC-

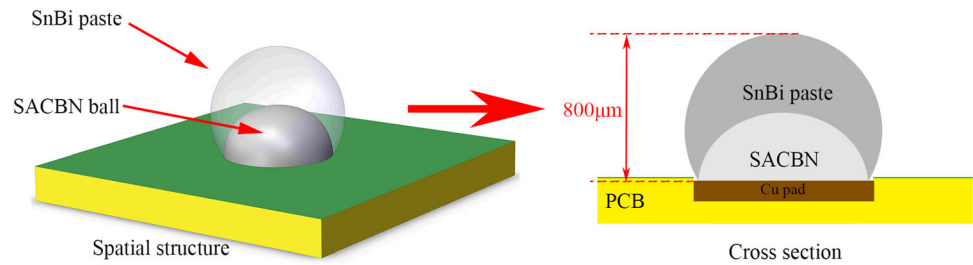
coated joints displayed higher shear strength and through-solder ductile failure. In our previous work [20], the SAC bump was pre-soldered on Cu to work as an interlayer between SnBi and Cu. The microstructure and mechanical properties of the solder joint were studied. It was found that the addition of the SAC bulk suppressed the brittle failure of the SnBi solder joint. However, the shear strength of the solder joint showed a decreasing trend.

According to our previous research, SACBN/Cu solder joint has excellent mechanical properties [21]. To improve the comprehensive performances of SnBi solder joints, SACBN solder was pre-soldered on a Cu pad and then SnBi/SACBN/Cu composite solder joints were obtained. The microstructure, hardness, shear strength, and fracture mode of the solder joints under different soldering times are investigated in this study.

2 Experimental procedures

Commercial Sn_{0.7}Ag_{0.5}Cu_{3.5}Bi_{0.05}Ni (SACBN) solder balls and eutectic Sn₅₈Bi solder paste were the solder materials used in this study. The melting temperatures of SnBi and SACBN solder were 139 °C and 220 °C, respectively. The soldering substrate was copper pad with a diameter of 640 μm on the printed circuit board (PCB). Firstly, the PCB was placed in anhydrous alcohol and cleaned with ultrasonic for 10 min. Secondly, the SACBN balls with a diameter of 450 μm were soldered by a heating platform at 260 °C for 70 s. Then the soldering samples were cooled to room temperature and were cleaned with an ultrasonic cleaner. The SnBi solder paste was dispensed evenly onto the SACBN/Cu joint by the Create-PSD solder paste dispenser. Next, the samples were heated to 160 °C for 40 s, 160 s, and 280 s, respectively, to obtain the SnBi/SACBN/Cu composite solder joints. The schematic diagram of the composite solder joint is shown in Fig. 1. For comparison, SnBi solder paste was heated at 160 °C for 40 s, 160 s, and 280 s, respectively, to obtain the SnBi/Cu solder joints with the same size of SnBi/SACBN/Cu. The height of both kinds of solder joints is 800 μm. For microstructure observation, cross-sectional samples were prepared by mounting, grinding, polishing, and etching. The microstructural morphology of the solder joints was observed by scanning electron microscope (SEM). Meanwhile, energy-

Fig. 1 Schematic diagram of the SnBi/SACBN/Cu solder joint



dispersive X-ray spectroscope (EDS) was used to determine the element distribution. The thickness of the IMC was calculated in Photoshop using the area method. Using the scale as a reference, the mean value of the thickness was calculated through the pixels of the area and length of the IMC layers. The shear experiment was carried out by the RESCH PTR-1000 bond tester. The shear height was set as 45 μm and the shear speed was 0.1 mm/s. The morphology of the shear fracture was observed by SEM. The hardness of the solder bulk was evaluated with a SHIMADZU DUH-211S indenter. Each solder bump had been tested at 10 locations to obtain the average hardness. The loading force and holding time of the hardness test were set to 100 mN and 10 s.

3 Results and discussion

3.1 Microstructure of the solder joints

Figure 2 shows the microstructure of the SnBi solder bulks with different soldering times. According to the previous study, the microstructure of the solder bulks is mainly composed of the white Bi-rich phase and the gray $\beta\text{-Sn}$ phase. This is supported by the EDS result in Fig. 2d. As shown in Fig. 2a, the solder bulk presents a dense network structure when the soldering time is 40 s. At the same time, the uniformity of the microstructure is low, and obvious composition segregation can be observed. As the soldering time increases, the microstructures in Fig. 2b and c become more uniform. The composition segregation is suppressed significantly. Meanwhile, the Bi-rich and $\beta\text{-Sn}$ grains show a clearly growing tendency. It is known that atoms undergo an intense thermal motion in molten alloys during the soldering process. Therefore, extending soldering time promotes the uniformity of the solder composition and facilitates the grain growth in the solder bulk.

Figure 3 presents the SEM micrographs and element mapping of Cu in the SnBi/Cu solder joints with the soldering time of 40, 160, and 280 s, respectively. Due to the interaction between SnBi solder and Cu pad, a very thin Cu_6Sn_5 interfacial IMC layer forms at the soldering interface as shown in Fig. 3a. As the soldering time increases, the thickness of the interface IMC shows an increasing trend. According to the element mapping results, obvious diffusion of Cu can be observed from the Cu pad into the solder bulk during the soldering process. The driving force for the diffusion is the concentration gradient of Cu at the interfacial area. As the soldering time extends, such diffusion becomes more intense. Consequently, the Cu_6Sn_5 interfacial IMC layer is much thicker when the soldering time reaches 280 s, as presented in Fig. 2c. In addition, those Cu_6Sn_5 grains present a dendritic morphology embedded with the Bi-rich grains. Compared with the other area in the solder bulk, the morphology of the Bi-rich phases is similar. The difference is that the $\beta\text{-Sn}$ and Bi-rich eutectic microstructure is replaced by the Cu_6Sn_5 and Bi-rich microstructure. It can be seen that the diffusion of Cu increases the concentration of Cu in the molten alloy near the interface. Since Cu and Bi have almost no interaction under these conditions, Cu reacts with Sn and forms Cu_6Sn_5 phase during the reaction. Meanwhile, the Bi element in the liquid alloy is precipitated as a Bi-rich phase.

Figure 4 shows the cross-sectional morphology and element mapping results of the SnBi/SACBN/Cu solder joint with the soldering time of 40 s. As shown in Fig. 4a, the solder joint includes three parts, SnBi, SACBN, and Cu pad. Meanwhile, these parts have two interfaces, which are SnBi/SACBN and SACBN/Cu. Three selected areas in Fig. 4a are magnified and are shown in Fig. 4b–d, respectively.

As shown in Fig. 4b, the SnBi area is composed of $\beta\text{-Sn}$ and Bi-rich phases. Compared with the SnBi/Cu solder joint in Fig. 2a, the microstructures of SnBi

Fig. 2 Microstructures and EDS analysis of SnBi solder bulks on Cu with different soldering times. **a** 40 s, **b** 160 s, **c** 280 s, **d** EDS of the point in **a**

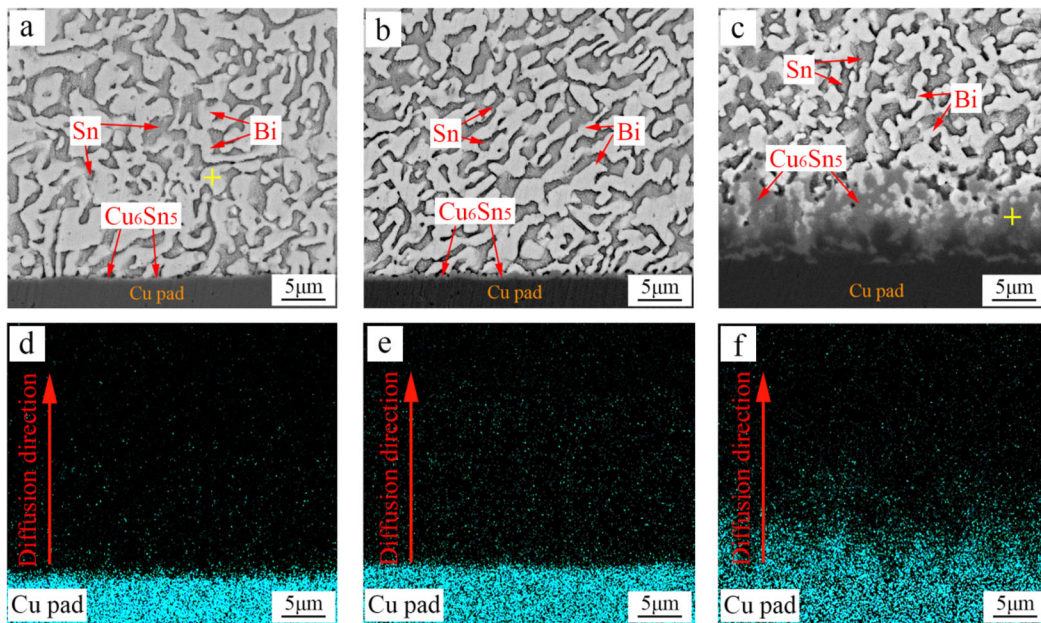
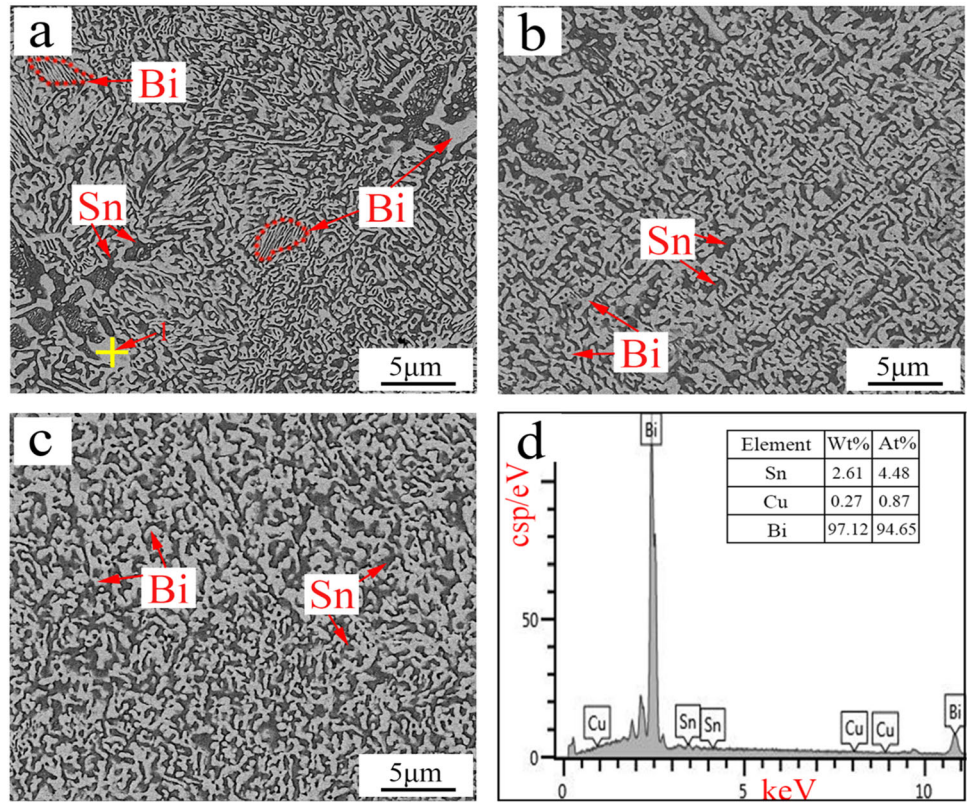


Fig. 3 Interfacial IMC and element mapping of Cu in SnBi/Cu solder joints under the soldering time of **a** and **d** 40 s, **b** and **e** 160 s, **c** and **f** 280 s

bulks in the composite solder joints are quite different. Based on the morphology and element mapping results in Fig. 4d–i, it can be seen that element diffusion occurs at the interface between the SACBN

bulk and the SnBi bulk. On one hand, Sn atoms diffuse from the SACBN bulk into the SnBi bulk during the second soldering process. The concentration of Sn in the molten SnBi is increased, and the SnBi eutectic

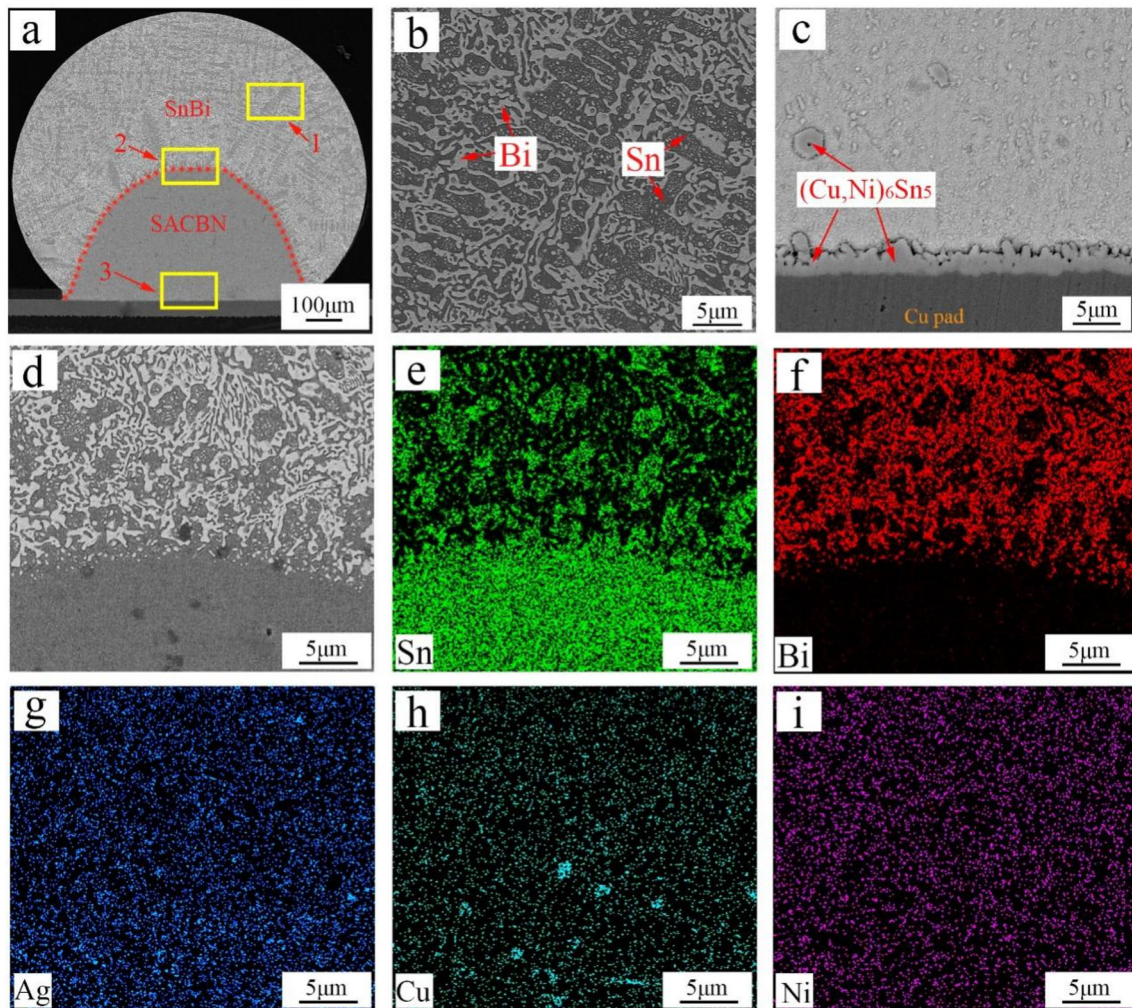


Fig. 4 Microstructure and element mapping of the SnBi/SACBN/Cu solder joint with the soldering time of 40 s. **a** Cross-sectional view of the joint, **b** magnified view of the area 1 in **a**, **c** magnified

view of the area 3 in **a**, **d** magnified view of the area 2 in **a**, and **e–i** element mapping of **d**

composition transforms to a hypereutectic composition. During the cooling stage, the β -Sn precipitating phase is formed in dendrites, as shown in the figure. On the other hand, regardless of the impact of the testing noise on the results, it can be seen that a trace amount of Ag, Cu, Ni elements diffuse from the SACBN bulk into SnBi, which also has a certain impact on its microstructure. However, due to the low content of these elements, such effect is relatively insignificant, and they usually exist as small IMC grains. Figure 4c shows the enlarged morphology of the SACBN/Cu interface. It is clear that when the SnBi soldering time is 40 s, the interfacial IMC is $(\text{Cu}, \text{Ni})_6\text{Sn}_5$ in the SnBi/SACBN/Cu solder joint. Compared with the SnBi/Cu solder joint in Fig. 3, the interface IMC and microstructure of the solder bulk

are changed due to the addition of the SACBN solder bulk.

Figure 5 shows the microstructure and element mapping of the SnBi/SACBN/Cu solder joint with the soldering time of 280 s. As shown in Fig. 5a, it has a similar structure with the solder joint soldered for 40 s in the second soldering stage as presented in Fig. 4a. However, the area of the SACBN bulk decreases with the increase of soldering time. The increasing soldering time stimulates the diffusion of atoms from the SACBN bulk into the molten SnBi alloy during the second soldering process. This phenomenon further increases the Sn content in the SnBi alloy, resulting in the formation of more β -Sn dendrites distributing in the SnBi bulk as shown in Fig. 5a. Meanwhile, the grain size of β -Sn in the SnBi

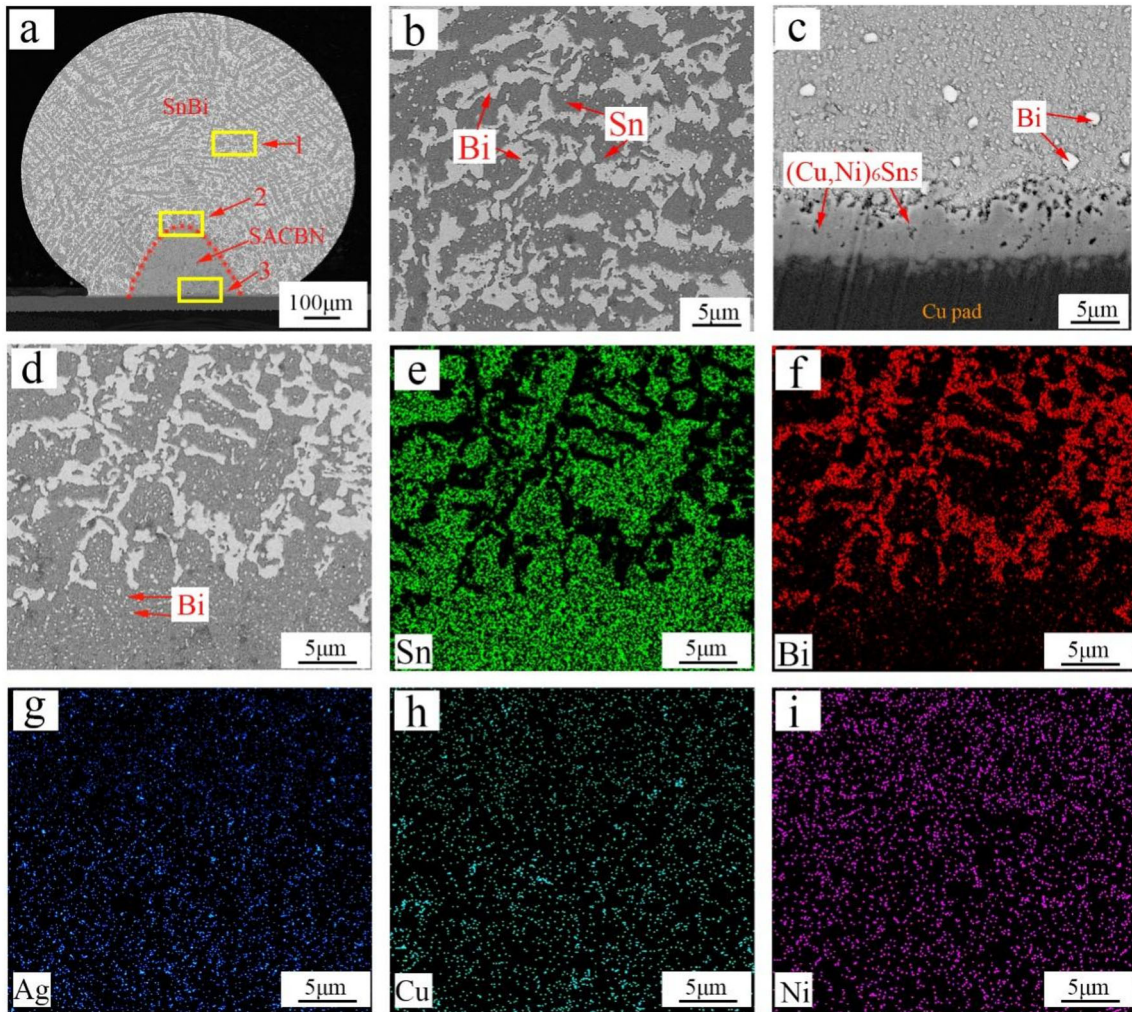


Fig. 5 Microstructure and element mapping of the SnBi/SACBN/Cu solder joint with the soldering time of 280 s. **a** cross-sectional view of the joint, **b** magnified view of the area 1 in **a**, **c** magnified

view of the area 3 in **a**, **d** magnified view of the area 2 in **a**, and **e–i** element mapping of **d**

bulk increases, as presented in Fig. 5b. In Sn–Bi binary system, when the concentration of Sn increases in the alloy with a hypereutectic composition, the liquidus temperature increases and thus promotes the growth of the β -Sn grains. According to the element mapping in Fig. 5d–i, increasing soldering time facilitates the diffusion of other elements at the SnBi/SACBN interface. Among them, Bi element diffuses from the SnBi alloy into the SACBN bulk. As shown in Fig. 5c, obvious Bi-rich particles can be observed near the SACBN/Cu interface. In addition, the $(\text{Cu}, \text{Ni})_6\text{Sn}_5$ IMC layer at the SACBN/Cu interface is getting thicker due to the increasing soldering time. The dominant factor is that the second soldering process accelerates the diffusion between SACBN

and Cu, which in turn promotes the growth of the interfacial IMC layer.

Figure 6 presents the IMC thickness in the solder joints. It can be seen from the figure that the interfacial IMC thickness of SnBi/SACBN/Cu is higher than that of SnBi/Cu under the same soldering time. According to the microstructures of the two solder joints, the interfacial IMC of SnBi/SACBN/Cu is a $(\text{Cu}, \text{Ni})_6\text{Sn}_5$ compound formed by the interfacial reaction of SACBN and Cu at 260 °C. Compared with the Cu_6Sn_5 at the SnBi/Cu interface, $(\text{Cu}, \text{Ni})_6\text{Sn}_5$ has more nucleation particles and forms a thicker IMC layer. In addition, the SnBi eutectic alloy has a large amount of Bi-rich grains, which hinder the diffusion of Sn and Cu and suppress the growth of Cu_6Sn_5 at the SnBi/Cu interface. It is also a factor for the

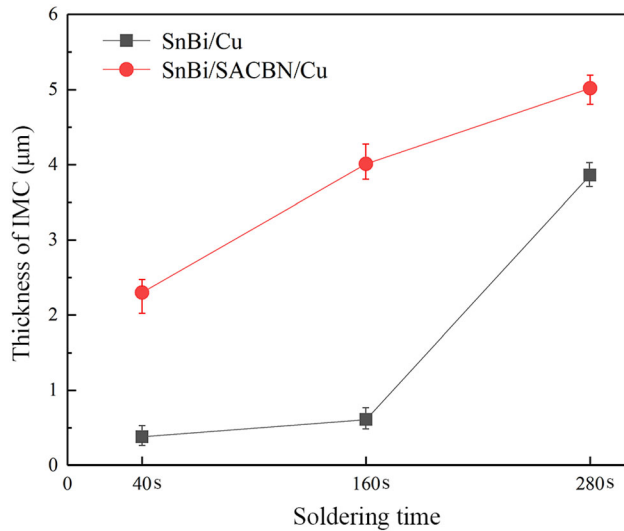


Fig. 6 IMC thickness of the solder joints

thickness of SnBi/SACBN/Cu IMC to be larger than SnBi/Cu. Besides, as presented in the figure, the IMC layers in the two kinds of solder joints increase. However, the growth mechanisms of the two are different. The formation and growth of the interfacial IMC layer in SnBi/Cu are mainly based on the liquid–solid diffusion between the molten SnBi alloy and the Cu pad. In contrast, in SnBi/SACBN/Cu solder joints, the IMC layer is formed during the soldering process of SACBN/Cu bumps and then grows due to solid–solid diffusion at the SACBN/Cu interface during the second soldering stage.

3.2 Mechanical properties of the solder joints

Figure 7 shows the average hardness of the two kinds of solder joints with the soldering time of 40 s, 160 s, and 280 s, respectively. The indentation area is the center of the SnBi part in the solder joints. The average hardness of the SnBi/Cu solder joints with a soldering time of 40 s is 418.3 MPa. The hardness decreases to 390.5 MPa and 338.2 MPa when the soldering time is 160 s and 280 s, respectively. Meanwhile, the average hardness of the SnBi bulks in the SnBi/SACBN/Cu solder joints is 350.2 MPa, 309.5 MPa, and 284.3 MPa, respectively. It can be seen that the hardness of the SnBi bulks in the two solder joints decreases as the soldering time increases. According to the previous analysis on the microstructure, increasing soldering time leads to the increase of the grain sizes of the two types of solder

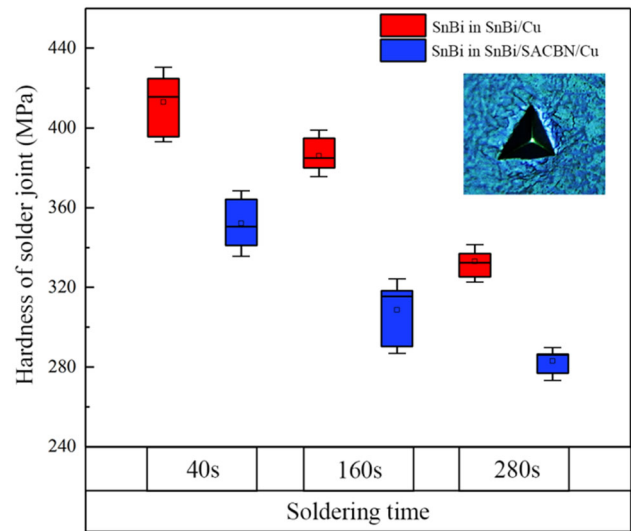


Fig. 7 Hardness of the SnBi solder bulks

joints, which is one of the reasons for the decrease of their hardness. In addition, for SnBi/SACBN/Cu solder joint, the diffusion of Sn from SACBN into SnBi increases its Sn content and facilitates the formation of large-size β -Sn grains. Therefore, the hardness of SnBi in SnBi/SACBN/Cu is lower than that in SnBi/Cu under the same soldering time. As the soldering time increases, such diffusion is promoted. This is also a key factor that decreases the hardness of the SnBi bulks in the SnBi/SACBN/Cu solder joints as the soldering time increases.

Figure 8 shows the shear strength of the two kinds of solder joints. The average shear strength of the SnBi/Cu solder joints with the soldering time of 40 s,

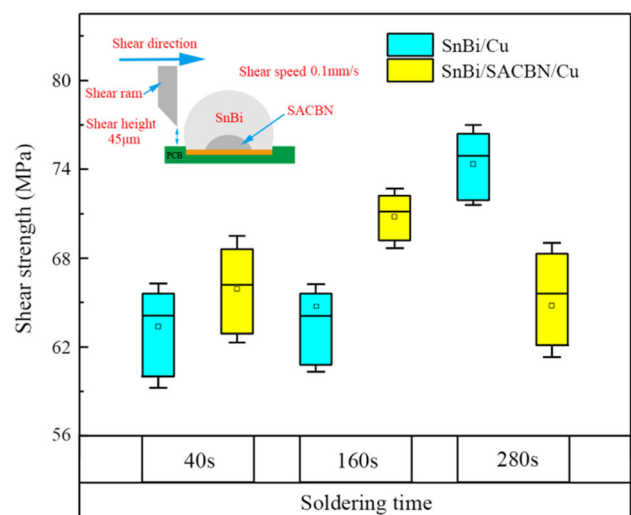


Fig. 8 Shear strength of the solder joints

160 s, and 280 s is 63.7 MPa, 64.8 MPa, and 75.4 MPa, respectively. Meanwhile, the average shear strength of the SnBi/SACBN/Cu solder joints with the soldering time of 40 s, 160 s, and 280 s is 66.1 MPa, 71.4 MPa, and 65.2 MPa, respectively. With the increase of soldering time, the shear strength of SnBi/Cu and SnBi/SACBN/Cu appears in different trends. Due to the high concentration of Bi in the SnBi eutectic solder, a large amount of Bi-rich grains generate and are located on the interfacial IMC layer. The growth of the IMC layer is suppressed and presents a thin and flat morphology in the solder joint. The extension of the soldering time stimulates the interfacial diffusion between the molten SnBi solder and the Cu pad. As shown in Fig. 3, more Cu atoms diffuse into the SnBi solder bulk because of the increasing soldering time. It has a positive effect on improving its mechanical performance. Therefore, the shear strength of the SnBi/Cu solder joints increases with the increase of the soldering time.

Figure 9 shows the shear fracture morphology and element mapping of the SnBi/Cu solder joints. It can

be seen from the figure that the fracture position of the three solder joints is all in the SnBi bulks near the SnBi/Cu interface. According to the shear morphology in Fig. 9a–c and the element mapping in Fig. 9g–i, it can be seen that as the soldering time increases, the fracture position tends to extend toward the interface. This phenomenon is consistent with the previous analysis. It shows that the diffusion of Cu into the solder bulk can improve its strength. In addition, this strengthening suppresses the deformation of the solder bulks and appears increasingly in brittle features during the shear process, as shown in Fig. 9d–f.

The shear strength of the SnBi/SACBN/Cu solder joint increases as the soldering time increases from 40 to 160 s but decreases when the soldering time reaches 280 s. Based on the analysis of microstructure, increasing soldering time promotes the elemental diffusion from SACBN into SnBi. It has a significant impact on the fracture mode of the solder joint as is shown in Fig. 10. When the soldering time is 40 s, as shown in Fig. 10a and g, the shear fracture

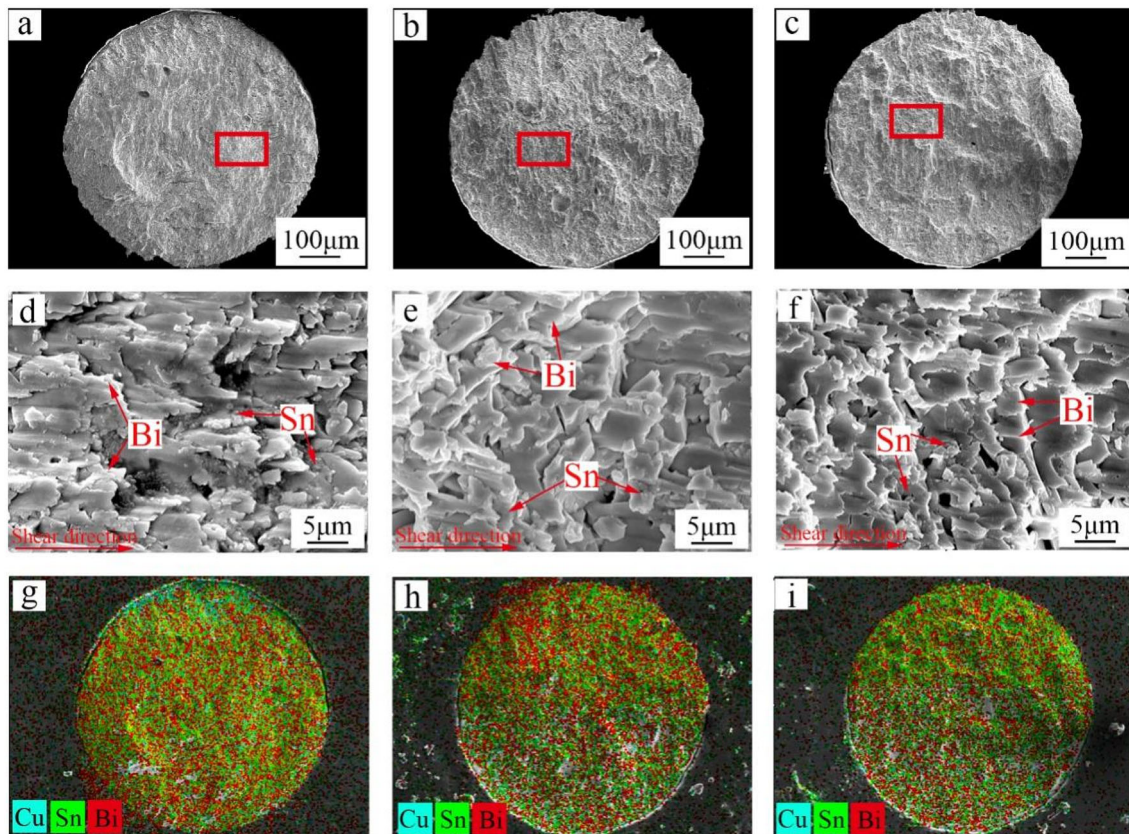


Fig. 9 Shear fracture and element mapping of the SnBi/Cu solder joints with the soldering time of a, d, and f 40 s, b, e, and h 160 s, c, f, and i 280 s

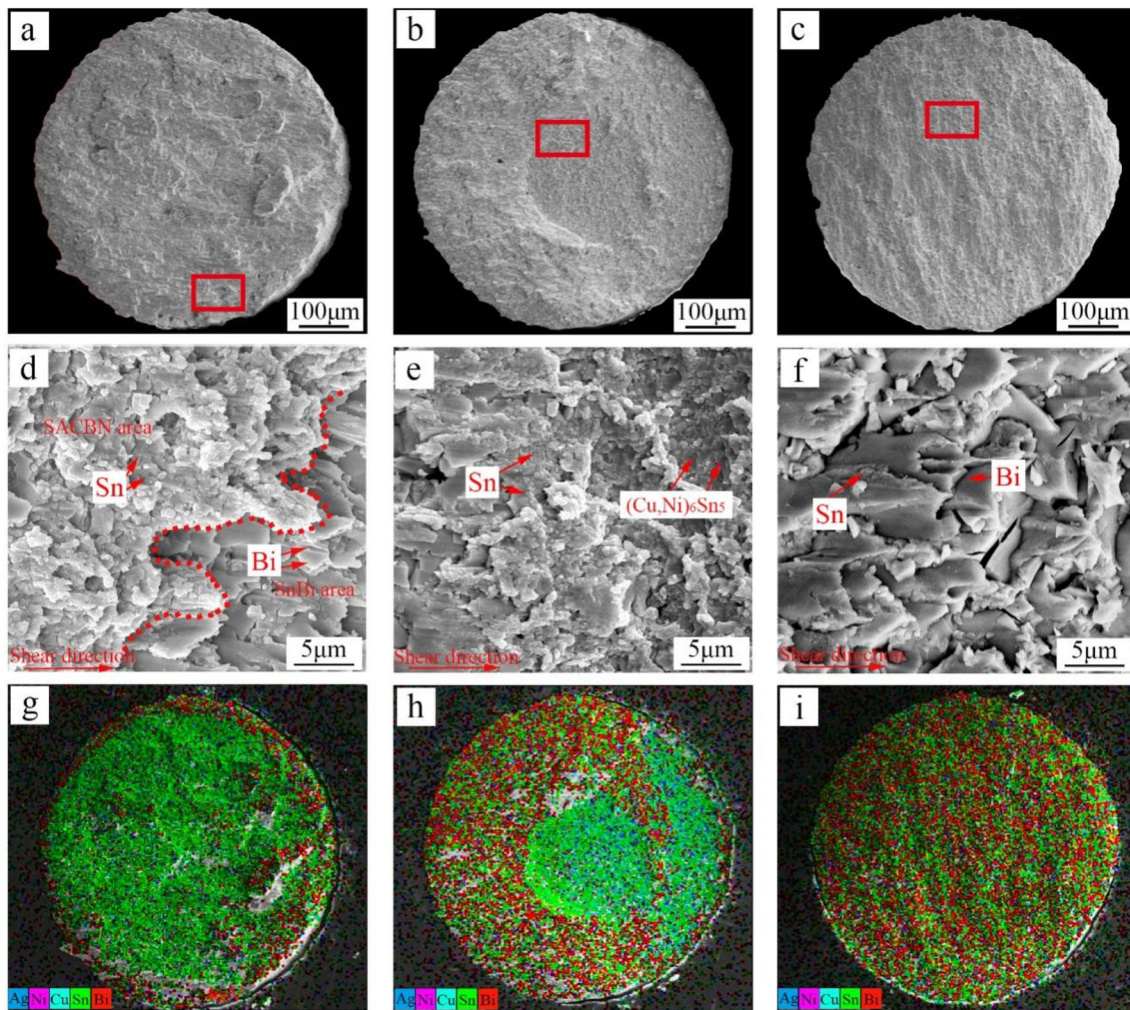


Fig. 10 Shear fracture and element mapping of the SnBi/SACBN/Cu solder joints with the soldering time of **a, d, and f** 40 s, **b, e, and h** 160 s, **c, f, and i** 280 s

is mainly located in SACBN bulk. Bi can only be detected at the edge of the fracture. As shown in Fig. 10d, where this area is partially enlarged, the microstructure of SACBN and SnBi can be observed. It can be deduced that the fracture generates in the SnBi bulk at the edge of the solder joint, and then propagates into the SACBN bulk during the shearing process. When the soldering time is increased to 160 s, the SACBN bulk further diffuses into the SnBi bulk, leading to the transformation of the fracture mode, as shown in Fig. 10b. According to the element mapping in Fig. 10h, the fracture surface is mainly composed of SnBi alloy and interfacial IMC, which can be observed in the magnified view in Fig. 10e. It is clear that the diffusion of SACBN does not only

lead to the microstructural transformation of the SnBi bulk but also affects the crack propagation in the solder joint. Consequently, the shear strength of the solder joint increases when the soldering time reaches 160 s. As shown in Fig. 10c, f, and i, when the soldering time increases to 280 s, SACBN diffuses in a large amount, and the crack is completely inside the SnBi bulk. Therefore, the enhancement of the SACBN bulk is suppressed since it has a limited effect on crack propagation, and thus the shear strength is reduced. According to the results and discussion, it can be summarized that soldering time has a significant impact on the shear strength and fracture mode of the SnBi/SACBN/Cu solder joints.

4 Conclusions

1. The SACBN bump diffuses into SnBi in the SnBi/SACBN/Cu solder joint during the soldering process, which changes the composition of the liquid SnBi alloy, thereby affecting the microstructure and mechanical properties of the solder joint.
2. The growth of the $(\text{Cu}, \text{Ni})_6\text{Sn}_5$ interfacial IMC in SnBi/SACBN/Cu solder joint is mainly based on solid–solid diffusion. Its growth rate is lower than that of the IMC based on liquid–solid diffusion in SnBi/Cu.
3. Increasing soldering time promotes the diffusion of SACBN into SnBi. The geometric size of the SACBN bulk in the SnBi/SACBN/Cu solder joint has a significant effect on its shear strength and fracture mode.
4. With the optimization of soldering time, the addition of SACBN bulk can improve the mechanical properties of SnBi solder joint.

Author contributions

YL: conceptualization, methodology, investigation, and writing—review & editing. JC: investigation, writing—original draft. YX: supervision. RC: investigation. HL: review & editing. SZ: review & editing. XZ: supervision.

Funding

The authors declare that no funds, grants, or other support were received during the preparation of this manuscript.

Data availability

The datasets generated during and/or analyzed during the current study are available from the corresponding author on reasonable request.

Declarations

Conflict of interest The authors have no relevant financial or non-financial interests to disclose.

References

1. G. Ren, I.J. Wilding, M.N. Collins, Alloying influences on low melt temperature SnZn and SnBi solder alloys for electronic interconnections. *J. Alloy. Compd.* **665**, 251–260 (2016)
2. Y. Liu, B. Ren, M. Zhou, X. Zeng, F. Sun, Microstructure, mechanical, and thermal behaviors of SnBi/Cu solder joint enhanced by porous Cu. *J. Mater. Sci-Mater. El.* **31**, 8258–8267 (2020)
3. Z. Lai, D. Ye, Microstructure and properties of Sn-10Bi-xCu solder alloy/joint. *J. Electron. Mater.* **45**, 3702–3711 (2016)
4. Y.A. Shen, S. Zhou, J. Li, C.H. Yang, S. Huang, S.K. Lin, H. Nishikawa, Sn-3.0 Ag-0.5Cu/Sn-58Bi composite solder joint assembled using a low-temperature reflow process for PoP technology. *Mater. Des.* **183**, 108144 (2019)
5. X. Zhao, M. Muraoka, M. Saka, Length-dependent electromigration behavior of Sn58Bi solder and critical length of electromigration. *J. Electron. Mater.* **46**, 1287–1292 (2017)
6. L. Zhao, Z. He, Z. Wang, L. Su, X. Lu, Simulation and experimental investigation on active thermography test of the solder balls. *IEEE. T. Ind. Inform.* **16**, 1617–1624 (2019)
7. C. Wu, J. Shen, C. Peng, Effects of trace amounts of rare earth additions on the microstructures and interfacial reactions of Sn57Bi1Ag/Cu solder joints. *J. Mater. Sci. Mater. El.* **23**, 14–21 (2012)
8. J. Shen, C. Wu, S. Li, Effects of rare earth additions on the microstructural evolution and microhardness of Sn30Bi0.5Cu and Sn35Bi1Ag solder alloys. *J. Mater. Sci. Mater. El.* **23**, 156–163 (2012)
9. D.L. Ma, P. Wu, Effects of Zn addition on mechanical properties of eutectic Sn-58Bi solder during liquid-state aging. *Trans. Nonferr. Metal. Soc.* **25**, 1225–1233 (2015)
10. W. Zhu, W. Zhang, W. Zhou, P. Wu, Improved microstructure and mechanical properties for SnBi solder alloy by addition of Cr powders. *J. Alloy. Compd.* **789**, 805–813 (2019)
11. Z. Wang, Q.K. Zhang, Y.X. Chen, Z.L. Song, Influences of Ag and In alloying on Sn-Bi eutectic solder and SnBi/Cu solder joints. *J. Mater. Sci. Mater. El.* **30**, 18524–18538 (2019)
12. S.Y. Zhao, Z.H. Cai, Y.P. Zhang, Y.H. Zhang, Effect of Sb doping on microstructure and mechanical properties of tin-bismuth near-eutectic solder. *Welding Technology.* **39**, 47–50 (2010)
13. X. Hu, H. Qiu, X. Jiang, Effect of Ni addition into the Cu substrate on the interfacial IMC growth during the liquid-state reaction with Sn-58Bi solder. *J. Mater. Sci. Mater. El.* **30**, 1907–1918 (2019)

14. L. Yang, S. Ma, G. Mu, Improvements of microstructure and hardness of lead-free solders doped with Mo nanoparticles. *Mater. Lett.* **304**, 130654 (2021)
15. S.M. Lee, J.W. Yoon, S.B. Jung, Interfacial reaction and mechanical properties between low melting temperature Sn–58Bi solder and various surface finishes during reflow reactions. *J. Mater. Sci. Mater. El.* **26**, 1649–1660 (2015)
16. W.R. Myung, Y. Kim, S.B. Jung, Evaluation of the bondability of the epoxy-enhanced Sn-58Bi solder with ENIG and ENEPIG surface finishes. *J. Electron. Mater.* **44**, 4637–4645 (2015)
17. J. Kim, W.R. Myung, S.B. Jung, Effects of aging treatment on mechanical properties of Sn-58Bi epoxy solder on ENEPIG-surface-finished PCB. *J. Electron. Mater.* **45**, 5895–5903 (2016)
18. H.F. Zou, Q.K. Zhang, Z.F. Zhang, Interfacial microstructure and mechanical properties of SnBi/Cu joints by alloying Cu substrate. *Mater. Sci. Eng. A* **532**, 167–177 (2012)
19. F. Wang, D.Y. Li, Z.J. Zhang, Improvement on interfacial structure and properties of Sn-58Bi/Cu joint using Sn-30Ag-05Cu solder as barrier. *J. Mater. Sci. Mater. El.* **28**, 19051–19060 (2017)
20. Y. Liu, R. Xu, H. Zhang, F. Sun, Microstructure and shear behavior of solder joint with Sn58Bi/Sn3.0Ag0.5Cu/Cu superposition structure. *J. Mater. Sci. Mater. El.* **30**, 14077–14084 (2019)
21. Y. Liu, J. Chang, M. Zhou, Y. Xue, X. Zeng, F. Sun, Microstructure and shear behavior of Sn58Bi/Cu solder joint enhanced by SnAgCuBiNi bump. *Mod. Phys. Lett. B* **34**, 2050413 (2020)

Publisher's Note Springer Nature remains neutral with regard to jurisdictional claims in published maps and institutional affiliations.